

Vehicle Longitudinal Speed Estimation Using 3DOF Localization Information and Genetic Solver

Reza Ghahremaninejad¹^a, Kerem Par¹^b, Ali Ufuk Peker²^c and Ömer Konan¹^d

¹ADASTEC, Istanbul, Turkey

²

{reza, kerem, ali, omer}@adastec.com

Keywords: Vehicle Velocity Estimation, Longitudinal Velocity Estimation, Genetic Solver, Optimization Problem.

Abstract: The accurate vehicle longitudinal speed measurement is vital for many sub-modules of current vehicle control units. Ego velocity estimation in Automated Vehicles (AV) scope is one of the fundamental functionalities required to properly operate many sub-modules like control, planning, and perception. The current speed sensors on most commercial vehicles have different precision and failure rates. To mitigate the faulty behavior of AV modules in vehicle speed sensor failure scenarios, a real-time velocity estimation method can play a redundant role in the vehicle speed sensor. This work attempts to estimate vehicle longitudinal speed having 3DOF real-time localization data. Considering the vehicle dynamic bicycle model, an objective function is formulated, and then a genetic solver solves the single objective optimization problem. The validation of the velocity estimation is discussed by comparing the real-time estimated value with accurate vehicle speed sensor measurement. Results show an acceptable recall of ego longitudinal velocity for redundancy application.

1 INTRODUCTION

The benefits of Automated Vehicle (AV) applications have been proven over the past years, and different AV applications are currently deployed in various regions. One of the core requirements for the successful deployment and operation of AVs is to have robust and safe AV software and hardware suites. To properly operate fundamental tasks of AV such as control, planning, and perception, AV hardware includes sensor suites such as LiDARs, cameras, RADARs, speed sensors, etc. The expected behavior of the AV highly depends on the sensor readings, where failure in sensing can cause AV failure. Classifying driving tasks as mission-critical, the immediate need to mitigate sensor failure scenarios, especially for the Society of Automotive Engineers (SAE) level-4 and higher Automated Driving Systems (ADS), gains attention. As mentioned in (Cassel et al., 2020), SAE level-4 and higher autonomy level vehicles are expected to detect the failure and respond autonomously to bring the vehicle into a safe state. A redundant source for sensor

reading would be of great value in performing such a failure detection. Equipping AVs with redundant sensors can be a solution despite increasing the cost of the vehicle hardware. Even though from a safety perspective, equipping some AV hardware with redundant units is the best practice, especially if the unit is an actuator, not a sensor, in some sensor cases, an estimation of sensor reading can be calculated to enable sensor reading failure detection reducing hardware cost by relatively low increase in computation cost. An example of efforts to address sensor failures in AV scope can be found in (Matos et al., 2024), (Safavi et al., 2021), and (Goelles et al., 2020).

Among different sensors, longitudinal speed sensors on today's commercial vehicles are one of the essential and crucial units. Ego velocity estimation using Visual Odometer (VO) (Khan and Adnan, 2017), (Wu et al., 2017) and (Pillai and Leonard, 2017) or LiDAR Odometer (LO), (Kwon et al., 2025) and (Clavijo et al., 2022) or using an Inertial Measurement Unit (IMU), and location displacement data over time is addressed among researchers (Saadeddin et al., 2014) and (Wang et al., 2011).

Some researchers consider vehicle motion and dynamic models to estimate ego states such as longitudinal speed (Jin et al., 2019). For instance, the author in (Fazekas et al., 2020) uses GNSS and IMU

^a <https://orcid.org/0000-0003-3766-6319>

^b <https://orcid.org/0000-0002-0659-6189>

^c <https://orcid.org/0000-0003-1332-0305>

^d <https://orcid.org/0009-0003-0909-5114>

measurements to estimate uncertain parameters accompanying wheel encoder sensor readings to calibrate wheel encoder odometry for localization purposes. They formulate the system uncertainly identification as a regression problem. Authors in (Hsu and Chen, 2012) used 6DOF localization information and two road angles to identify real-time vehicle dynamics. The model can then calculate vehicle states, including vehicle longitudinal velocity. Similar to the work of (Hsu and Chen, 2012), localization data is used in the present work. Rather than estimating a model uncertainly similar to (Fazekas et al., 2020) and (Hsu and Chen, 2012) to obtain accurate vehicle dynamics, the 3DOF localization data here is used to directly estimate the vehicle longitudinal velocity.

The present work estimates ego vehicle longitudinal velocity using 3DOF localization data: Cartesian position X-axis, Y-axis, and rotation around Z-axis, heading on the map frame. To do so, the vehicle dynamic bicycle model is considered to formulate an optimization problem. The Single Objective Optimization Problem (SOOP) is later solved by a Genetic Algorithm (GA)- based solver. A time-series data set containing vehicle longitudinal sensor measurements and 3DOF localization information of KARSAN Autonomous e-ATAK, an 8-meter, level-4 automated bus, is used for validation. The e-ATAK, automated by ADASTEC Corp. flowride.ai® full stack AV software, currently operating in Stavanger, Norway, as a public transportation means for six hours per day, five days per week, performing an average of 60 km per day. The data is recorded onboard using the Flowride® logger, an onboard AV data recording module (Par et al., 2024). Using 3DOF localization data, estimated velocity is obtained by solving the optimization problem. The accuracy of the estimated value is discussed by comparing results with vehicle onboard sensor measurement.

The optimization problem formulation is presented in detail in the following section. Section 3 is dedicated to validating the estimated value over the e-ATAK dataset. Finally, a conclusion to the present work and possible extensions are discussed.

2 PROBLEM FORMULATION AND APPROACH

This section is organized into two subsections. First, problem formulation is discussed and formulated as a SOOP. Later, the second subsection presents a GA-based solver architecture to solve the SOOP.

2.1 Formulation

3DOF real-time localization data is used as measurement and is expressed as $\langle X_{loc}(t), Y_{loc}(t), \theta_{loc}(t) \rangle$ where $X_{loc}(t)$, $Y_{loc}(t)$ and $\theta_{loc}(t)$ are ego vehicle base frame position on the map frame X-axis and Y-axis in meter and orientation around Z-axis, heading in *rad* respectively. From the vehicle dynamic bicycle model, to find the same information position on the map frame, the following equation is realized:

$$\begin{aligned}\hat{X}(t) &= dt[V_x(t) \cos \theta_{loc}(t - dt) - V_y(t) \sin \theta_{loc}(t - dt)] \\ &\quad + X_{loc}(t - dt) \\ \hat{Y}(t) &= dt[V_x(t) \sin \theta_{loc}(t - dt) + V_y(t) \cos \theta_{loc}(t - dt)] \\ &\quad + Y_{loc}(t - dt) \\ \hat{\theta}(t) &= dt\hat{\theta}(t) + \theta_{loc}(t - dt)\end{aligned}\quad (1)$$

where $\hat{X}(t)$, $\hat{Y}(t)$ and $\hat{\theta}(t)$ are the position of the ego vehicle and its heading on the map frame at time t respectively, considering information position from localization at time $t - dt$. $\hat{\theta}(t)$, the heading change rate is obtained as follows:

$$\hat{\theta}(t) = aC_f(\delta V_x - V_y) \cos \delta + \frac{bC_r V_y}{(C_r b^2 + C_f a^2) \cos \delta}\quad (2)$$

In real-time operation, dt is the time difference between the current time when the last location data is received and the time stamp of the previous location data. Having a 40 Hz localization calculation rate adding delays in the estimation calculation, the following inequality can be expressed: $dt > 0.025$ seconds.

$V_x(t)$, $V_y(t)$ and $\delta(t)$ are values to estimate in the present work, which are ego vehicle longitudinal and lateral velocities in *m/s* and front wheel angles in *rad* respectively. a and b are vehicle base frame distance with front and rear axels. C_f and C_r are front and rear tire stiffness. The values of a, b, C_f and C_r are parameters to this problem and are set according to the KARSAN e-ATAK vehicle. The problem statement is to find $V_x(t)$, $V_y(t)$ and $\delta(t)$. Using 3DOF localization information at $t - dt$ the position information from the vehicle dynamic bicycle model, $\hat{X}(t)$, $\hat{Y}(t)$ and $\hat{\theta}(t)$ is obtained. Later, comparing with the location data at time t ; $X_{loc}(t)$, $Y_{loc}(t)$ and $\theta_{loc}(t)$, an error value can be calculated as follows:

$$\begin{aligned}er_X(t) &= (\hat{X}(t) - X_{loc}(t))^2 \\ er_Y(t) &= (\hat{Y}(t) - Y_{loc}(t))^2 \\ er_\theta(t) &= (\hat{\theta}(t) - \theta_{loc}(t))^2\end{aligned}\quad (3)$$

Theoretically considering localization error neglectable, a right estimation of values for $V_x(t)$, $V_y(t)$ and $\delta(t)$ would minimize summation of the errors. To that end, an objective function can be constructed using weighted summation of errors as follows:

$$\min \bar{e} = w_x er_X(t) + w_y er_Y(t) + w_\theta er_\theta(t) \quad (4)$$

2.2 Approach

GA-based method to solve SOOP is a common practice among researchers (Katoch et al., 2021). To minimize equation (4), by estimating right solution vector, $S = \langle V_x(t), V_y(t), \delta(t) \rangle$, the following chromosome vector is defined: $ch_n = \langle V_{xn}, V_{yn}, \delta_n, fit_n \rangle$. A container vector holding a randomly generated chromosome population is defined as $pop = \langle ch_1, ch_2, \dots, ch_{P_s} \rangle$. The random chromosome is generated by assigning uniform random values between the minimum and maximum values of each gene:

- $\min_{v_x} < V_x < \max_{v_x}$
- $\min_{v_y} < V_y < \max_{v_y}$
- $\min_\delta < \delta < \max_\delta$

First, at the beginning of the solving approach, an initial pop set with the size of P_s is generated with random genes, then the fitness score for each chromosome is calculated according to equations (1) to (4). Half of the best chromosomes with lower fitness values will be selected later, and the rest will be removed from pop set, resulting in a set with a size of $P_s/2$ ready for cross-over and mutation operation. In cross-over, two random chromosomes are selected from pop as parents: $ch_k, ch_j \in pop$ to offspring child chromosome as follows:

$$\begin{aligned} ch_{child} = & \langle \alpha V_{xk} + \beta V_{xj}, \\ & \alpha V_{yk} + \beta V_{yj}, \\ & \alpha \delta_k + \beta \delta_j \rangle \end{aligned} \quad (5)$$

where α is a random value between 0 and 1 and $\beta = 1 - \alpha$. The ch_{child} then will be added to the pop set. The cross-over operation continues till the size of pop reaches P_s , meaning the iteration count for the cross-over operation is equal to $P_s/2$. A mutation operation will be performed on pop as a final GA operation. Random values of γ_x, γ_y and γ_δ where $\gamma_{x,min} < \gamma_x < \gamma_{x,max}$, $\gamma_{y,min} < \gamma_y < \gamma_{y,max}$ and $\gamma_{\delta,min} < \gamma_\delta < \gamma_{\delta,max}$ will be added to V_{xl}, V_{yl} and δ_l of $ch_l \in pop$ if $\sigma < M$ where σ is random value between 0 and 1 and M is mutation rate which is parameter to mutation operator. This will finalize one genetic

population evaluation step. The number of Genetic Evaluation iteration GE , M , P_s , \min_{v_x} , \min_{v_y} , \min_δ , \max_{v_x} , \max_{v_y} , \max_δ , w_x , w_y and w_θ are parameters to presented method and will be discussed in the evaluation step in details. Figure 1 summarizes the genetic population evaluation cycle.

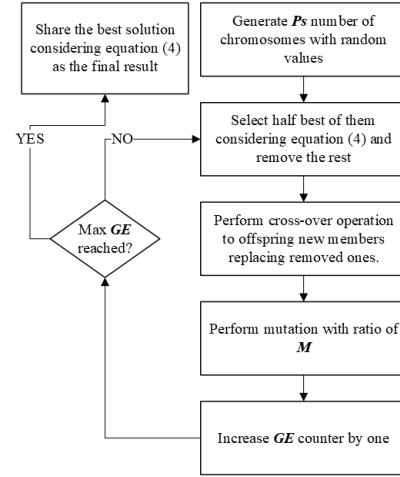


Figure 1: GA solver to estimate V_x, V_y and δ .

3 RESULTS AND VALIDATION DISCUSSION

To validate the formulation and GA solver, one of the logged data of the e-ATAK automated bus operating at Stavanger, Norway, is used. Figures 2, 3, and 4 represent ego vehicles' trajectory on map frame in meters, heading in rad , and velocity in m/s .

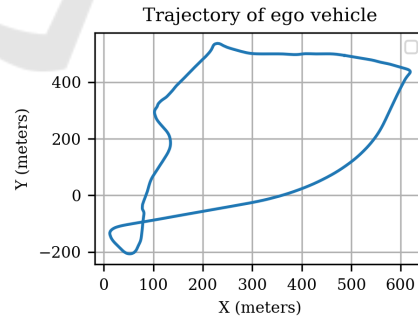


Figure 2: Ego vehicle trajectory from localization.

Table 1 presents parameters with constant values selected experimentally to present here. Results for different values of P_s and GE are presented to study the GA solver performance in real-time considering experiment hardware configuration. Table 2 shows details of the experiment computer for reference. In real-time operation, increasing P_s and GE increases GA solver computation load resulting in increasing

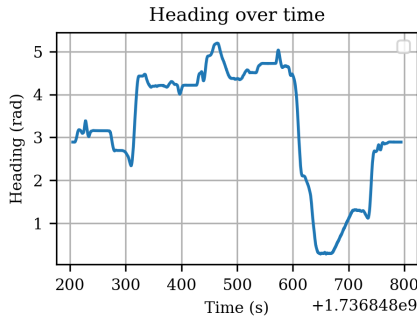


Figure 3: Ego vehicle heading.

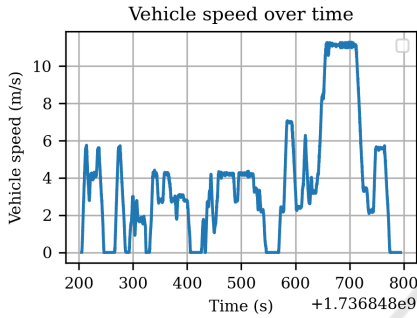


Figure 4: Ego vehicle speed.

evaluation execution time. On the other hand, increasing P_s and GE will result in better estimation of the V_x , V_y and δ_x . Figure 5 shows the comparison of vehicle longitudinal velocity measured from the sensor versus the estimated values where $P_s = 800$ and $GE = 200$ as example. Tables 3, 4 and 5 show result of all experiments with different $GE = 100, 200, 400$ and $P_s = 400, 800, 1200$. The success of each configuration is measured by the calculation of absolute error of estimated value compared with sensor reading in the form of error recall at $< 0.5m/s$, $< 1m/s$, $< 2m/s$ and $< 5m/s$: $r@0.5$, $r@1$, $r@2$ and $r@5$. Average Execution Time (AET) for each GE step is also noted in ms to assess the performance of each configuration in real-time application.

Table 1: Constant parameters for the present experiment.

Parameter	Value
M	0.01
min_{v_x}	-3 m/s
min_{v_y}	-1.5 m/s
min_{δ}	-0.5 rad
max_{v_x}	18 m/s
max_{v_y}	9 m/s
max_{δ}	0.5 rad
w_x	10^6
w_y	10^6
w_{θ}	10^4

Table 2: The experiment computer configuration.

Operating System	Ubuntu 20.04 LTS
CPU	Core i7, 8th Gen, 12-core
RAM	16 GByte DDR4

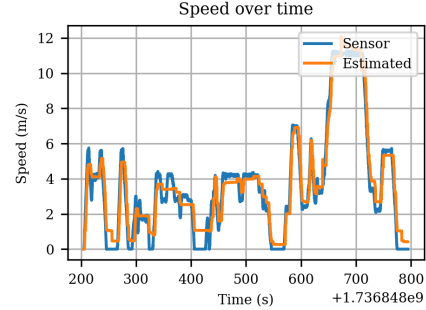


Figure 5: Ego vehicle estimated speed versus measured speed from the sensor.

The calculated longitudinal velocity from Displacement Over Time (DOT) is compared with the proposed method. Displacement over two consecutive localization data obtained as follows:

$$\begin{aligned} d_x &= X_{loc}(t) - X_{loc}(t - dt) \\ d_y &= Y_{loc}(t) - Y_{loc}(t - dt) \end{aligned} \quad (6)$$

Then, for ego longitudinal velocity:

$$V_x = \frac{\sqrt{d_x^2 + d_y^2}}{dt} \quad (7)$$

Figure 6 shows the calculated speed using DOT versus sensor readings. DOT's highly noisy velocity estimation can be addressed using low-pass filters such as the Moving Average Filter (MAF). The effect of MAF with different window sizes is also shown, which indicates improving the speed estimation; however, low pass filters such as MAF impose latency on the measurement. Having 40 Hz localization data, the time difference between two consecutive location data will be 25 ms. The latency introduced by MAF with window size of w will be $25w/2$ ms (Smith, 1997). Table 6 constructed for DOT results with different MAF windows. Instead of AET, the latency introduced by MAF is indicated to assess real-time application performance.

Different approaches could be selected from the results shown in Tables 3 to 6 considering the prime objective of this work, to provide redundancy to vehicle speed sensors. This selection will depend on more details of the ADS module's ego vehicle speed accuracy requirement from being close enough to real-time and tolerable deviation from real velocity perspectives. For instance, in ADS with a 10 Hz perception rate, latencies and AETs around 100 ms can

Table 3: The experiment result with $P_s = 400$.

GE	r@0.5	r@1	r@2	r@5	AETms
100	4.2%	22.2%	42.7%	84.7%	17.9
200	13.2%	29%	61.1%	100%	32.8
400	51.1%	83%	100%	100%	67

 Table 4: The experiment result with $P_s = 800$.

GE	r@0.5	r@1	r@2	r@5	AETms
100	19.9%	37%	79%	100%	36.1
200	54.4%	80.1%	100%	100%	66.9
400	98.6%	99.9%	100%	100%	129.6

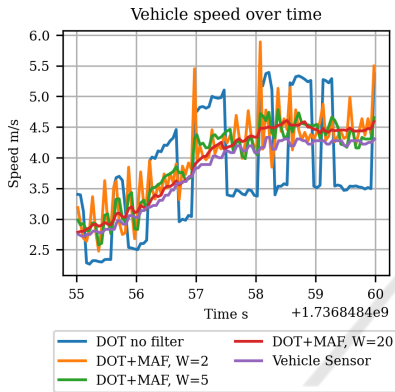


Figure 6: Ego vehicle calculated velocity using DOT with different windows size of MAF.

be considered acceptable. Based on this assumption, configurations at Table 4 with $P_s = 800$ and $GE = 400$, Table 5 with $P_s = 1200$ and $GE = 200$, also Table 6, using DOT with window size of 10 can be good candidates. The best performance belongs to configuration with $P_s = 1200$ and $GE = 400$, Table 5. The closest DOT accuracy is obtained with a window size of 20, which has less $r@0.5$ and the worst time performance. It is worth mentioning that the AET highly depends on computing configuration and can be improved with better hardware and software implementation. However, the latency imposed by MAF when using the DOT method is independent of computation resources.

4 CONCLUSION

The present work attempts to estimate vehicle longitudinal speed mainly to mitigate speed sensor failure cases, especially in the SAE level-4 ADS scope, which requires ADS to detect failures and perform fail-over maneuvers. To do so, a redundant velocity estimation method, which uses 3DOF localization data, is proposed. Ego longitudinal velocity is

 Table 5: The experiment result with $P_s = 1200$.

GE	r@0.5	r@1	r@2	r@5	AETms
100	29.9%	64.3%	97.3%	100%	49.9
200	89.3%	99.9%	100%	100%	102
400	99.2%	100%	100%	100%	201.9

Table 6: DOT raw results and MAF output with different windows size.

win	r@0.5	r@1	r@2	r@5	lat ms
1	38%	74%	93%	100%	0
2	89%	97%	99%	100%	25
5	90%	98%	100%	100%	62.5
10	93%	99%	100%	100%	125
20	92%	100%	100%	100%	250
50	86%	100%	100%	100%	625
100	69%	97%	100%	100%	1250
200	55%	80%	99%	100%	2500

estimated using a GA-based optimizer by solving a SOOP formulated considering the vehicle dynamic bicycle model. Different configurations of initial population and generation evaluation steps resulted in various performances of the method in real-time operation from execution time and the accuracy of estimation perspective. Estimation accuracy is measured by comparing it to the e-ATAK automated bus speed sensor. The DOT-based approach for vehicle longitudinal speed calculation is also presented to discuss the GA performance better, where the velocity calculation results improved using MAF. Different MAF window sizes were practiced, which validated the superiority of the proposed method compared to the results of DOT combined with MAF.

The formulation of the current work does not consider the accuracy of localization data. However, the deviation in the localization information can be included in formulating the objective function. Also, the present work does not study different implementations and configurations of cross-over and mutation operations. The effect of varying hardware configurations on the proposed method's performance is also not addressed in this work. All mentioned topics can be an extension of the present work. Adding other measurements next to 3DOF localization information and using other vehicle dynamic models in problem formulation can also be different extensions of this work.

ACKNOWLEDGEMENTS

This work results from collaborative effort and passion within the ADASTEC Corp. family.

REFERENCES

- Cassel, A., Bergenhem, C., Christensen, O. M., Heyn, H.-M., Leadersson-Olsson, S., Majdandzic, M., Sun, P., Thorsén, A., and Trygvesson, J. (2020). On perception safety requirements and multi sensor systems for automated driving systems. *SAE International Journal of Advances and Current Practices in Mobility*, 2(2020-01-0101):3035–3043.
- Clavijo, M., Jiménez, F., Serradilla, F., and Díaz-Álvarez, A. (2022). Assessment of cnn-based models for odometry estimation methods with lidar. *Mathematics*, 10(18):3234.
- Fazekas, M., Gáspár, P., and Németh, B. (2020). Identification of kinematic vehicle model parameters for localization purposes. In *2020 IEEE International Conference on Multisensor Fusion and Integration for Intelligent Systems (MFI)*, pages 373–380. IEEE.
- Goelles, T., Schlager, B., and Muckenhuber, S. (2020). Fault detection, isolation, identification and recovery (fdiir) methods for automotive perception sensors including a detailed literature survey for lidar. *Sensors*, 20(13):3662.
- Hsu, L.-Y. and Chen, T.-L. (2012). Vehicle dynamic prediction systems with on-line identification of vehicle parameters and road conditions. *Sensors*, 12(11):15778–15800.
- Jin, X., Yin, G., and Chen, N. (2019). Advanced estimation techniques for vehicle system dynamic state: A survey. *Sensors*, 19(19):4289.
- Katoch, S., Chauhan, S. S., and Kumar, V. (2021). A review on genetic algorithm: past, present, and future. *Multimedia tools and applications*, 80:8091–8126.
- Khan, N. H. and Adnan, A. (2017). Ego-motion estimation concepts, algorithms and challenges: an overview. *Multimedia Tools and Applications*, 76:16581–16603.
- Kwon, W., Lee, H., Kim, A., and Yi, K. (2025). Lidar-based odometry estimation using wheel speed and vehicle model for autonomous buses. *International Journal of Control, Automation, and Systems*, 23(1):41–54.
- Matos, F., Bernardino, J., Durães, J., and Cunha, J. (2024). A survey on sensor failures in autonomous vehicles: Challenges and solutions. *Sensors*, 24(16):5108.
- Par, K., Peker, A. U., Ghahremaninejad, R., Özcan, A., and Sahin, E. (2024). Introducing flowride@ logger, an on-board data collection framework for commercial automated vehicles. In *VEHITS*, pages 488–495.
- Pillai, S. and Leonard, J. J. (2017). Towards visual ego-motion learning in robots. In *2017 IEEE/RSJ International Conference on Intelligent Robots and Systems (IROS)*, pages 5533–5540. IEEE.
- Saadeddin, K., Abdel-Hafez, M. F., and Jarrah, M. A. (2014). Estimating vehicle state by gps/imu fusion with vehicle dynamics. *Journal of Intelligent & Robotic Systems*, 74:147–172.
- Safavi, S., Safavi, M. A., Hamid, H., and Fallah, S. (2021). Multi-sensor fault detection, identification, isolation and health forecasting for autonomous vehicles. *Sensors*, 21(7):2547.
- Smith, S. W. (1997). The scientist and engineer’s guide to digital signal processing. *California Technical Pub.*
- Wang, Y., Mangnus, J., Kostić, D., Nijmeijer, H., and Jansen, S. T. (2011). *Vehicle state estimation using GPS/IMU integration*. IEEE.
- Wu, M., Lam, S.-K., and Srikanthan, T. (2017). A framework for fast and robust visual odometry. *IEEE Transactions on Intelligent Transportation Systems*, 18(12):3433–3448.